Magn Reson Mater Phy (2009) 22:375–383
DOI 10.1007/s10334-009-0189-8

RESEARCH ARTICLE

3D T_1-mapping for the characterization of deep vein thrombosis

Ulrike Blume · James Orbell · Matthew Waltham · Alberto Smith · Reza Razavi · Tobias Schaeffter

Received: 28 May 2009 / Revised: 5 November 2009 / Accepted: 12 November 2009 / Published online: 28 November 2009

Abstract
Purpose The aim of this work was to investigate fast T_1-mapping for the characterization of deep vein thrombosis (DVT).
Methods The accuracy and reproducibility of the T_1-mapping sequence was tested in phantoms and in 8 healthy volunteers on a 1.5 T clinical scanner using a 32-channel array coil. Furthermore, the feasibility of the technique was tested in 5 patients diagnosed with DVT by measuring the volume and T_1 values of the thrombus at 5 time points over a period of 6 months.
Results The results of the phantom and volunteer study showed a high accuracy and reproducibility for the quantification of T_1. The resolution of the T_1-maps was high enough to identify small anatomical structures. T_1 values derived for normal blood and various other tissues were comparable to those reported in the literature. In all patients, the T_1 times of thrombi showed decreased values ($T_1 = 843 \pm 91$ ms) in the acute phase and recovered back to normal values of blood ($T_1 = 1{,}317 \pm 36$ ms) after 6 months.
Conclusions Measurement of all relevant T_1 values of acute thrombi and normal blood achieved accurate and reproducible results in vivo. Fast T_1 quantification of the thrombus can provide information about tissue characteristics such as thrombus resolution. Such a quantitative MRI technique may be valuable in studying the factors that influence natural resolution and in evaluating treatment effects that enhance this process.

Keywords T_1-mapping · Quantitative MRI · Deep vein thrombosis · DVT · Thrombus resolution

U. Blume (✉) · R. Razavi · T. Schaeffter
Division of Imaging Sciences, The Rayne Institute,
King's College London, St Thomas Hospital,
4th Floor Lambeth Wing, London SE1 7EH, UK
e-mail: Ulrike.blume@kcl.ac.uk

J. Orbell · M. Waltham · A. Smith
Academic Department of Surgery, Cardiovascular Division,
St Thomas Hospital, London, UK

U. Blume · J. Orbell · M. Waltham · A. Smith · R. Razavi · T. Schaeffter
NIHR Biomedical Research Centre at Guy's & St Thomas'
NHS Foundation Trust, London, UK

Introduction

Deep vein thrombosis (DVT) is a common disease with an occurrence of about 1:1,000 per year [1]. Detection of DVT is an important problem in clinical diagnosis. The widely accepted imaging method for DVT is contrast-enhanced venography [2]. However, this procedure requires cannulation of dorsal foot veins, resulting in patient discomfort and there is a risk of allergic reactions to the contrast material [3]. Duplex ultrasonography has become the initial diagnostic test of choice because of its accuracy, non-invasiveness, low cost and ease of use [4]. However, it has limited sensitivity for thrombi within the deep veins of the calf and pelvis [5]. Over the last decade, different magnetic resonance imaging (MRI) methods have been proposed to diagnose DVT with the use of gadolinium-based MRI contrast agents [6–9]. Three-dimensional (3D) gadolinium-enhanced MR-venography allows a comprehensive non-invasive evaluation of the deep venous system [8], but requires exact timing of the MR acquisition to catch the venous phase of the contrast agent passage [7]. MRI has also successfully been used for imaging DVT without the need for contrast agents [10–14]. One approach has been the use of an inflow sensitive multi-slice balanced steady-state free precession (bSSFP) sequence [14], showing thrombosis as a dark signal void surrounded by bright venous blood. Acute DVT can also be detected on T_1-weighted images. This technique is based upon the

presence of methemoglobin, which is formed from hemoglobin by oxidative denaturation to the ferric (Fe^{3+}) during the acute phase of DVT. Methemoglobin has paramagnetic properties resulting from its 5 unpaired electrons which results in shortening of the T_1 relaxation time [12,15]. In vitro studies have demonstrated that there is a linear relationship between the concentration of methemoglobin and T_1 shortening [16]. On T_1-weighted images, the contrast between the thrombus (bright) and surrounding tissues (dark) is generated. Previous studies have used this T_1-weighted imaging technique to detect thrombi [2,10–13,17–19]. The bright signal persists over several weeks and is thought to disappear due to the removal of red blood cells by macrophages as a part of the thrombus resolution [2,10,11,13,15], resulting in a decrease of the thrombus signal with time [20]. This relationship may be clinically important by differentiating acute DVT from chronic DVT. However, the signal intensity of T_1-weighted images depends strongly on the MRI sequence parameters, e.g., inversion time. This makes it difficult to quantify thrombus resolution based on T_1-weighted images only.

The measurement of the longitudinal relaxation time T_1 for each pixel (T_1-mapping) can provide additional information about thrombus characteristics such as the mechanism of in vivo methemoglobin generation, age, and regression. Different methodologies for the measurement of the longitudinal relaxation time T_1 have been published over the last decade. Depending on the clinical application, the total scan time, accuracy, and reproducibility are important parameters for choosing the most appropriate quantification mapping method. The gold standard to measure T_1 is the inversion recovery (IR) sequence [21], but this is often impractical due to the need for very long scan times. For clinical scans, the resulting data set has to cover a large volume with a good resolution and must be acquired with scan times of minutes. Therefore, different fast imaging quantification methods have been proposed in order to apply T_1-mapping to different pathologies. T_1 can be measured from the signal intensity of a spoiled gradient echo (SPGR) at multiple flip angles with a fixed TR [22–25]. While this approach permits the rapid acquisition of large volume T_1-maps, the accuracy and reproducibility of this technique strongly depends on the correct knowledge of the transmitted flip angle. Another fast T_1 quantification can be achieved by the implementation of a multipoint acquisition that samples the relaxation curve at multiple times after an initial inversion pulse, resulting in a considerably faster acquisition. This technique was first described by Look and Locker [26] and applied for imaging by Deichmann [27]. However, the measurement of long T_1 relaxation times like blood (T_1 = 1,200–1,441 ms [28,29]) with a 3D Look–Locker sequence is a challenging task in a clinical setting. Very long magnetization recovery delays as well as small flip angles are necessary to ensure accurate measurements.

The aim of this work was to investigate fast T_1-mapping for the characterization of DVT in vivo. The accuracy and reproducibility of the Look–Locker T_1-mapping technique was assessed in phantoms and volunteers, and the feasibility of the thrombus detection and quantification approach was tested in 5 patients diagnosed with acute DVT. The thrombus regression was analyzed by measuring changes over time in the longitudinal relaxation time T_1, and in the thrombus volume, using multislice bSSFP and 3D T_1-weighted fast gradient echo MRI sequences.

Materials and methods

Fast T_1 acquisition and calculation

Different fast T_1-mapping methods based on the Look–Locker sampling scheme [26] have been described by other researchers [27,30–34]. The method used in this work is based on the publication by Deichmann [27] and is illustrated in Fig. 1. After a non-selective adiabatic inversion pulse, the relaxation behavior of the longitudinal magnetization M_z is detected by a series of 24 gradient echo images. For each image along the longitudinal magnetization recovery curve, 8 k-space lines with a centric phase encoding order were acquired with a TR of 6.7 ms and a TE of 3.3 ms, which resulted in an acquisition window of 53.6 ms per image. A flip angle of 6° was used to minimize the perturbation of the longitudinal magnetization. The different inversion times ranged from 20 ms (shortest TI) up to 1,253 ms (longest TI). Furthermore, a long relaxation delay was employed after each acquisition to ensure magnetization recovery. The delay was chosen to be 4 s in order to allow tissues with very long relaxation times like blood (T_1 = 1,200–1,441 ms [28,29]) to recover 95% (for T_1 = 1,441 ms) to 98% (for T_1 = 1,200 ms) of their thermodynamic equilibrium. By using this Look–Locker technique, the longitudinal magnetization recovery behavior is determined by the effective longitudinal relaxation time T_1^* and approaches a saturation value M_0^* which is below the equilibrium value M_0. Therefore,

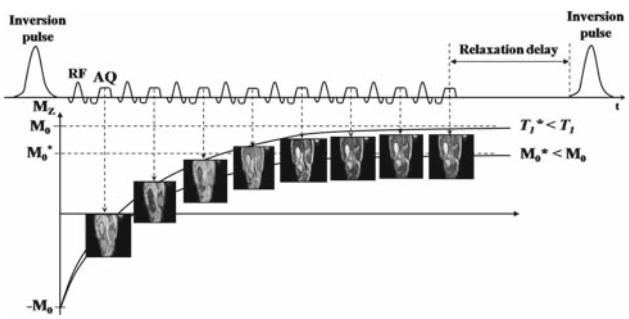

Fig. 1 Look–Locker pulse sequence scheme

Table 1 Summary of patient diagnoses, risk factors, and overview of MRI follow-up scans

Patient	Diagnosis DVT	Risk factors	MRI follow-up scans	Reason for termination of participation
A	Popliteal vein, no extension	None	Completed	None
B	Popliteal and femoral vein	None	Completed	None
C	Popliteal to mid femoral vein	Factor V Leiden, previous DVT in the same leg	Completed	None
D	Popliteal and femoral vein	Recent pneumonia and cholecystitis; antipopholipid syndrome	Completed	None
E	Popliteal and femoral vein	Existing malignancy	Uncompleted	Malignant melanoma

signal-time data was fitted to a three-parameter equation [31] which is given by

$$M_z(t) = M_0^* - \left(M_0 + M_0^*\right) \mathrm{e}^{-t/T_1^*} \quad (1)$$

T_1^* was calculated by using a least squares Levenberg–Marquardt curve-fitting algorithm. Afterward, a T_1 correction was performed with

$$T_1 = T_1^* \left(\frac{M_0 + M_0^*}{M_0^*} - 1\right). \quad (2)$$

Imaging

All imaging was performed on a 1.5 T clinical scanner (Philips Achieva) using a 32-channel receiver array coil (In vivo), allowing for wider anatomical coverage ($400 \times 400\,\mathrm{mm}^2$). This coil consists of an anterior and posterior unit, each with 16 independent coil elements arranged in two-dimensional arrays (4×4 grid arrays). The fast 3D Look–Locker T_1 quantification method was validated by phantom and volunteer experiments.

Phantoms

A phantom was made of 9 water-filled tubes with varying dilutions of gadolinium to give a broad range of T_1 values covering clinically relevant in vivo T_1 relaxation times (approximately 120–1,385 ms). A standard IR-sequence was used as a reference to validate the 3D Look–Locker sequence. It was performed with the following imaging parameters: 2D fast gradient echo acquisition, non-selective adiabatic inversion pulse, 8 mm slice thickness, FOV: $230 \times 230\,\mathrm{mm}^2$, matrix: 176×176, in-plane resolution: $1.3 \times 1.3\,\mathrm{mm}^2$, TR/TE = 3.6/1.8 ms, flip angle of 15°, 12 time points along the longitudinal relaxation curve, a segmented *k*-space acquisition with 8 readouts (acquisition window of 28.8 ms) after each inversion pulse, centric phase encoding order, and a range of inversion times: 20–2,000 ms including one without inversion pulse. The inversion pulse was applied every 10 s to ensure full magnetization recovery. The total measurement time resulted in 44 min for one slice. A three-parameter fit and a least squares Levenberg–Marquardt curve-fitting algorithm was used to generate a T_1-map.

The imaging parameters for the Look–Locker sequence are described earlier. Additional parameters were a 2D fast gradient echo sequence with a FOV of $230 \times 230\,\mathrm{mm}^2$, matrix size of 176×176, resolution of $1.3 \times 1.3\,\mathrm{mm}^2$, and a total scan time of 2 min. Furthermore, two T_1-maps were acquired to analyze the reproducibility of the Look–Locker sequence.

Volunteers

The fast T_1-mapping technique was applied to 8 healthy volunteers, and the resulting T_1 values of different tissues were compared with values from the literature. The volunteers were scanned twice on two different days to investigate the reproducibility using a Bland–Altman analysis. The study was approved by the local ethics committee, and written consent was obtained from all participants.

Patients

The legs of 5 patients (4 male, 1 female, average age: 56, age range: 29–73 years) with acute DVT diagnosed by duplex ultrasonography were imaged. All patients were placed feet-first in a supine position and both legs were imaged simultaneously. All patients had thrombosis arising in the popliteal vein with all but one having extension into their femoral vein proximally. Table 1 summarizes the diagnosis as well as additional risk factors of all patients. The first MR imaging was performed within 10 days (average of 9 days, range: 4–10 days) after the diagnosis of DVT. Scanning was repeated at least four more times until 6 months after the diagnosis of DVT (time points: 3 weeks, 1, 3, 6 months). After a survey and a coil-sensitivity scan, two different imaging sequences

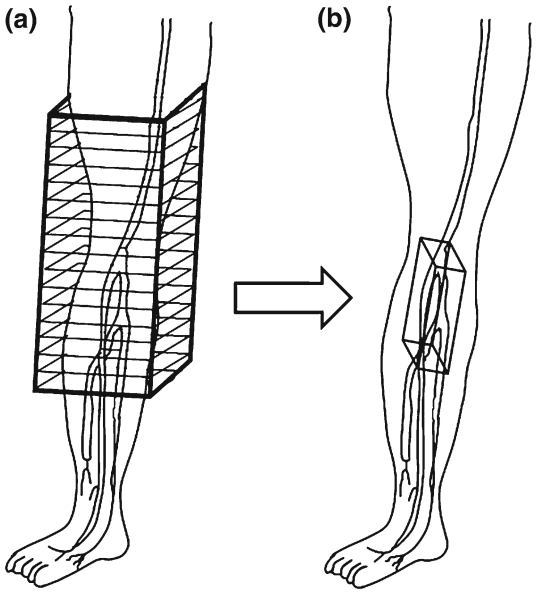

Fig. 2 Principles of the comprehensive sequence protocol. **a** Detection: global fast direct thrombi visualization of both legs, **b** quantification: local T_1 measurement of the whole thrombus

were chosen to detect the thrombus in a large field of view (FOV) without the need of contrast agent. After imaging and visual detection of the thrombus, the acquired data set was used to plan the location and orientation of the T_1-mapping sequence using a three-point planning tool (Fig. 2). The total scan time of the comprehensive DVT-imaging protocol was less than 20 min.

Detection of DVT

(a) A multislice balanced steady-state free precession (bSSFP) imaging sequence with a centric ordered k-space was used to acquire MR-venography images allowing the discrimination of stationary clot (dark) and flowing blood (bright) [14,35]. The imaging parameters were voxel size of $0.78 \times 0.78 \times 5\,\text{mm}^3$, an interslice gap of 0.5 mm, flip angle of 85°, 20 start-up cycles, TE = 2.7 ms, 70 slices and a balanced acquisition with a turbo factor of 24 and a TR of 5.4 ms. The scan time to acquire a volume of $200 \times 400 \times 385\,\text{mm}^3$ was 1:45 min. Due to only one phase-encoding direction (AP), a SENSE factor of 2 was applied.

(b) A magnetization-prepared 3D fast gradient echo sequence with a non-selective inversion RF-pulse was used for direct thrombus imaging [11,13]. The image acquisition was ECG-triggered and performed in end diastole when the flow in the femoral artery is slow [36]. The inversion time is dependent on the heart rate of the patient and was chosen such that the k-space center was sampled during the null point of blood (T_1 = 1,441 ms [29]). The inversion time was determined by Fleckenstein-equation [37]. Fat suppression was performed to improve image contrast. The imaging parameters were voxel size of $1.36 \times 1.36 \times 3.5\,\text{mm}^3$, flip angle of 30°, TE = 2.5 ms, 108 slices and multiple gradient echo acquisitions (32 readouts per cardiac cycle) with a repetition time of TR = 5.3 ms. The scan time to acquire a volume of $200 \times 400 \times 385\,\text{mm}^3$ was around 2 mins with a total SENSE factor of 4 (2 in AP and 2 in FH direction) depending on the heart rate. The detection of thrombi was considered positive (abnormal) for acute thrombosis if there was a high signal in the course of a deep vein, against a background in which the signal of fat and blood was suppressed.

Quantification of DVT resolution

After imaging and visual detection of the thrombus, the acquired data set was used to plan the location and orientation of the Look–Locker T_1-mapping sequence using a three-point planning tool (Fig. 2). Because the FOV needed to be adjusted for each patient, the image resolution of $1.25 \times 1.25 \times 1.25\,\text{mm}^3$ was kept constant for each scan. A 3D multipoint Look–Locker T_1-mapping sequence [26] always covered the whole thrombus in 10–21 slices. Due to a small volume thickness 12.5–26.0 mm of the sagittal angulated 3D slab, parallel imaging could only be applied to one phase-encoding direction (AP) with a factor of 2, which resulted in a total scan time between 5 and 12 min depending on the number of slices. An R_1-map ($R_1 = 1/T_1$) was displayed for each slice in order to highlight the thrombus in the resulting map.

Data analysis

For the phantom and volunteer data, homogeneous regions of interest (ROI) were chosen on the T_1-maps for each tube or in vivo tissue. A Bland–Altman [38] analysis was used to compare the T_1 variability between the fast Look–Locker T_1-mapping sequence and the conventional IR-method as well as the reproducibility of the fast Look–Locker T_1-mapping sequence. The coefficient of variation was defined as the standard deviation of the differences between the two different measurements divided by their mean, and expressed as a percentage.

For the patient feasibility study, all data from the three MR sequences (multislice bSSFP, 3D T_1-weighted fast gradient echo, and T_1-mapping) were used to measure the size of thrombus, so were analyzed slice by slice. In addition, the R_1 of the thrombus was also analyzed from each 3D T_1-map.

A ROI was chosen on each slice (Fig. 3), where the thrombus could be detected due to its positive (3D T_1-weighted fast

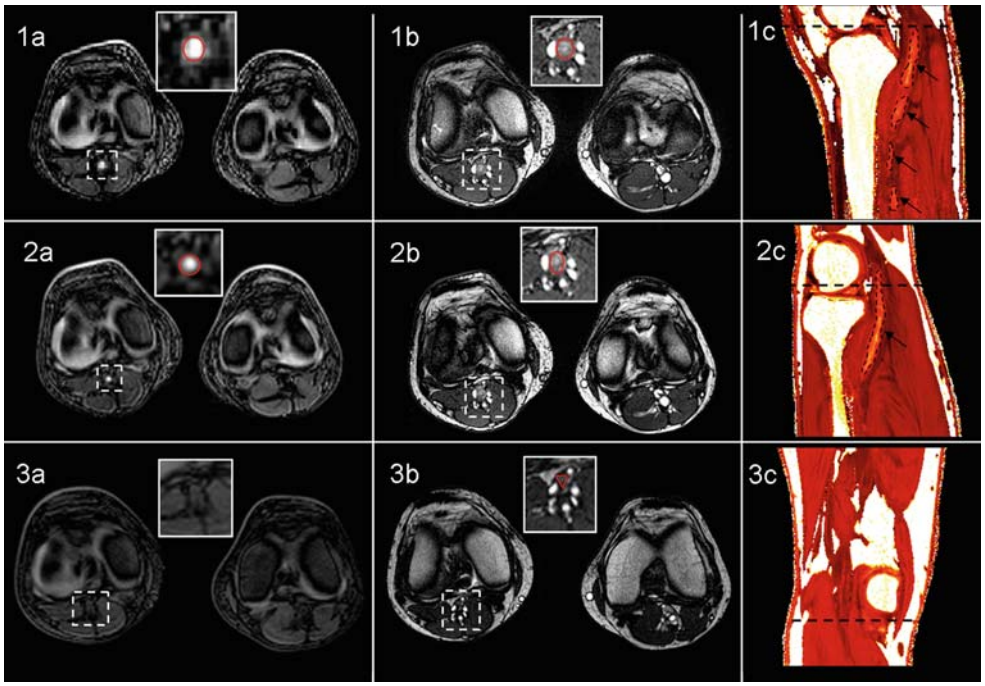

Fig. 3 Results of patient B at 10 days (*1 row*), 1 month (*2 row*), and 6 months (*3 row*) after the diagnosis. The first *two columns* show both legs in order to compare the signal intensity in both veins. *Column a*: transverse slice of 3D T_1-weighted fast gradient echo data set, *column b*: transverse slice of multislice bSSFP data set, *column c*: corresponding R_1-map with matching T_1 values: **1** $T_1 = 662 \pm 51$ ms, **2** $T_1 = 786 \pm 65$ ms, and **3** $T_1 = 1{,}356 \pm 67$ ms. The *smaller boxes* display a zoomed region of the same image showing the thrombus

gradient echo) or negative (multislice bSSFP) contrast to the surrounding tissue. The acute thrombus could be detected on the R_1-map as an area of increased R_1 values (i.e., short T_1 relaxation times) within the vein compared to the surrounding blood. The volume of the thrombus was also measured on the R_1-map by using a threshold approach. First, a ROI was placed within the vein where a significant increase of R_1 values could be detected. The mean values as well as the standard deviation of R_1 in the ROI were calculated. The threshold was calculated by the difference of the mean values and two standard deviations and used to define the volume. Only R_1 values higher than the calculated threshold were used to ensure that only pixels within the acute thrombus were selected. The resulting pixels were used to calculate the average R_1 value as well as the standard deviation and the total size of the thrombus.

Results

Phantoms and volunteers

Figure 4a summarizes the results of the phantom study to test the accuracy of the fast T_1 quantification in comparison with an inversion recovery sequence. The mean difference in the T_1 value using the conventional IR and the fast T_1- mapping sequence was 2.52% with a low coefficient of variation of 0.98%. The results of the interstudy variability of the fast T_1-mapping sequence are summarized in Fig. 4b–d. In healthy volunteers, the relaxation times of different areas (blood, skeletal muscle, and subcutaneous fat) were measured. The results of all the volunteers are shown in Table 2, which agree very well with the literature values [29,39]. The variation of T_1 in 8 healthy volunteers was 10 ms for skeletal muscle and 22 ms for blood.

Patients

The first MR examination was completed in all subjects without complications. The presence of DVT was confirmed with MRI in all patients. On all early scans, the 3D T_1-weighted fast gradient echo sequence allowed suppression of blood while acute thrombi were clearly visible as high-signal intensity structures. The location of the detected thrombus always matched with an area of dark signal intensity on the multislice bSSFP images. The four follow-up scans could only be performed in patient A, B, C, and D. Patient E could not attend the follow-up MR scans because of an existing malignancy.

Figure 3 shows a comparison of the three imaging sequences (T_1-weighted fast gradient echo, bSSFP, and an R_1-map) of one slice from patient B over time. The images of the first row were acquired at 10 days, the images of the

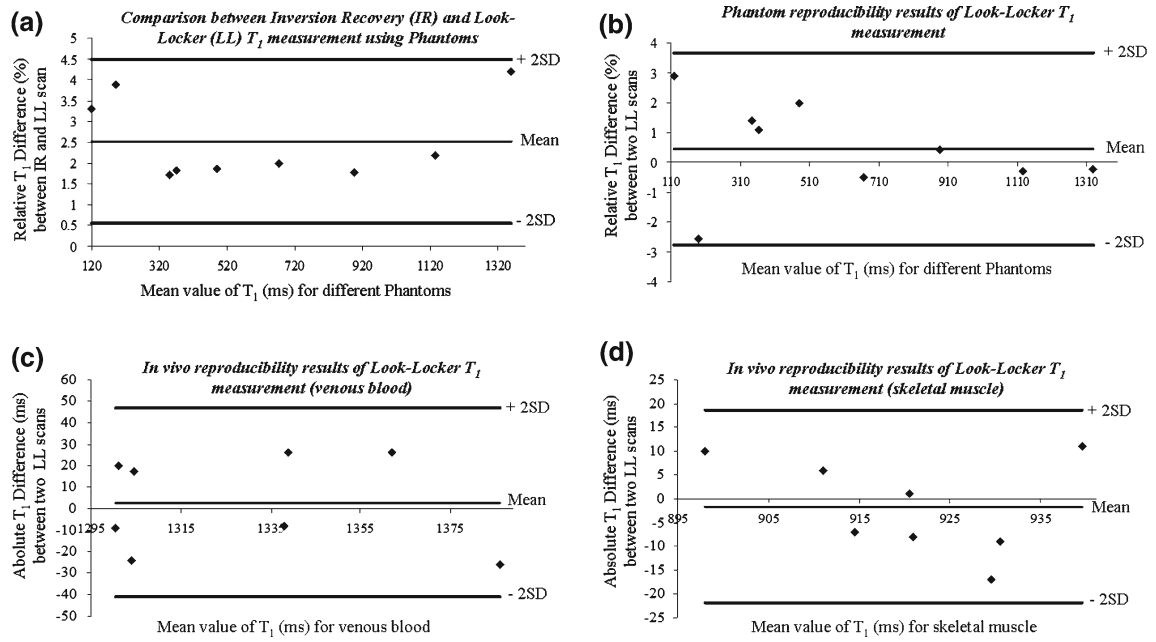

Fig. 4 Bland–Altman plots of differences between phantom T_1 measurements: **a** IR-based T_1-mapping sequence compared with Look–Locker-mapping sequence, **b**–**d** reproducibility of Look–Locker-mapping sequence: results of phantom (**b**) T_1 measurements, T_1 relaxation times of venous blood (**c**) and skeletal muscle (**d**) in healthy volunteers

Table 2 Comparison of measured T_1 relaxation times of 8 healthy volunteers to values from literature (references in brackets)

Tissue	T_1 (Look–Locker) (ms)	T_1 (Literature) (ms)
Blood	1,329 ± 33	1,441 ± 120 [28]
Skeletal muscle	920 ± 13	1,008 ± 20 [28]
Subcutaneous fat	277 ± 12	288 ± 8.42 [39]

second row at 1 month, and the final acquisition at 6 months after the diagnosis of DVT is shown in the last row. The three different imaging sequences are presented in three separate columns. The first two columns show the transverse slices of the two detection sequences (T_1-weighted fast gradient echo and bSSFP), where both legs are displayed in order to compare the signal intensity of both veins including the T_1-weighted gradient echo images in the first column and the multislice bSSFP images in the second column. In Fig. 3, 1a (10 days, T_1-weighted fast gradient echo), the thrombosis generates a high-signal intensity in comparison with the background tissues. After 1 month, however, the signal intensity and size of the thrombus decreased (Fig. 3, 2a) and finally disappeared after 6 months (Fig. 3, 3a). This correlates well with the quantitative analysis, which is described as R_1-maps in the third column (Fig. 3, 1c–3c). The images show that the thrombus can also be detected by increased R_1 values inside of the right popliteal vein (Fig. 3, 1c and 2c). The T_1 values of the thrombus at positions corresponding to the slice in Fig. 3 were (1a) $T_1 = 662 \pm 51$ ms, (2a) $T_1 = 786 \pm 65$ ms, and (3a) $T_1 = 1{,}356 \pm 67$ ms, respectively. The results of the second detection sequence (multislice bSSFP) are shown in the second column (Fig. 3, 1b–3b). Due to the imaging principle of this sequence, the negative contrast on these images inside the right popliteal vein indicates an occlusion or slow flowing blood. However, after 6 months (Fig. 3, 3b), dark contrast inside the vein was still noticeable.

In all 4 patients, the analysis of the bSSFP images always resulted in the largest thrombus volume which remained for much longer compared to the 3D T_1-weighted fast gradient echo images and the T_1-maps. Figure 5 also shows a difference between volumes determined by T_1-weighted and T_1-mapping sequence.

The results of all 4 patients are summarized in Fig. 5. Over time, the measured thrombus volume decreased on all 3 imaging sequences. The corresponding T_1 relaxation times of thrombi (mean: $T_1 = 843 \pm 91$ ms, range : $T_1 = 552$–$1{,}130$ ms) were less than normal blood ($T_1 = 1441$ ms [29]). After 6 months, the T_1 relaxation time recovered back to the normal T_1 relaxation time of blood (mean $T_1 = 1{,}317 \pm 36$ ms). The results of the thrombus size also varied between the three imaging sequences (T_1-weighted fast gradient echo, multi slice bSSFP, T_1-mapping).

In Fig. 6, a comparison between the T_1-weighted fast gradient echo detection sequence and the quantitative R_1-maps is shown over time. The results were acquired from patient A with a thrombus in the left popliteal vein at 10 days

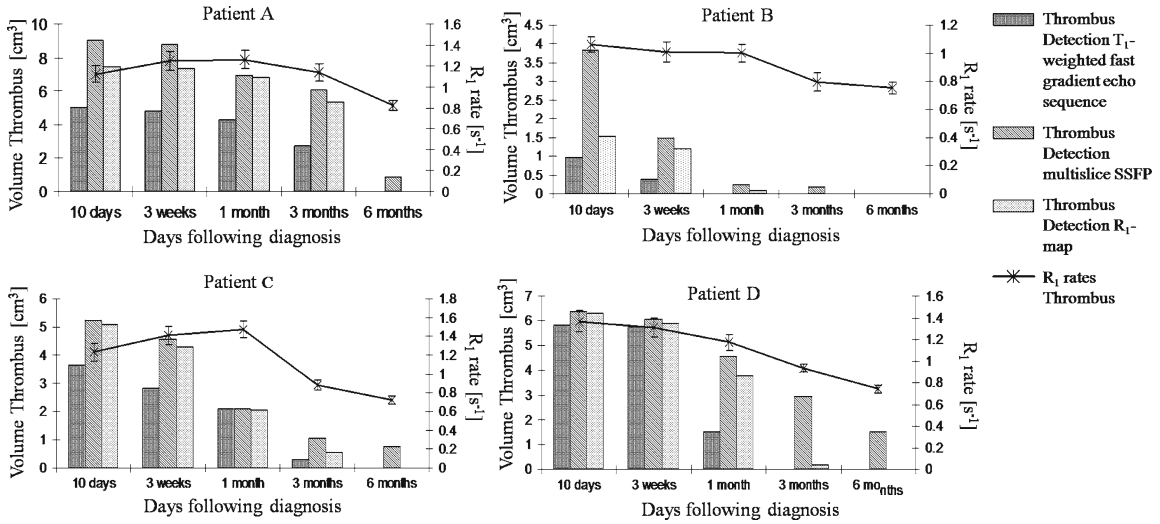

Fig. 5 Summary of patient results: change of thrombi size and R_1 relaxation rate over time

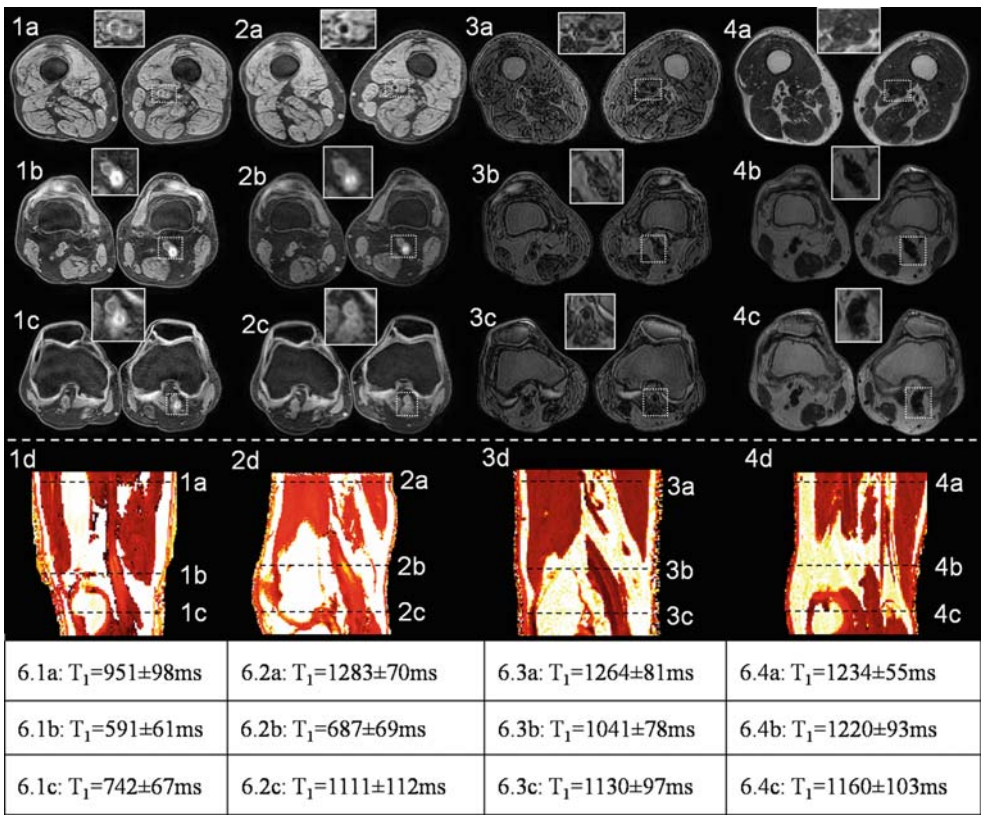

6.1a: T_1=951±98ms	6.2a: T_1=1283±70ms	6.3a: T_1=1264±81ms	6.4a: T_1=1234±55ms
6.1b: T_1=591±61ms	6.2b: T_1=687±69ms	6.3b: T_1=1041±78ms	6.4b: T_1=1220±93ms
6.1c: T_1=742±67ms	6.2c: T_1=1111±112ms	6.3c: T_1=1130±97ms	6.4c: T_1=1160±103ms

Fig. 6 Results of patient A at 10 days (**1a–c**), 3 weeks (**2a–c**), 3 months (**3a–c**), and 6 months (**4a–c**) days after the diagnosis. For each time point, one slice of the corresponding R_1-map is shown in the *fourth row* (*1d, 2d, 3d, 4d*), and three transverse slices of T_1-weighted 3D data set at different levels through the thrombus including corresponding T_1 values are displayed. The *smaller boxes* display a zoomed detail of the same image showing the thrombus

(1 column), 3 weeks (2 column), 3 months (3 column), and 6 months (4 column). Three transverse slices of the T_1-weighted 3D data set are shown in the first three rows. In all these images (Fig. 6, 1a–c), the signal from blood in the right popliteal vein is suppressed as a result of the inversion time. On the left leg, however, the three slices demonstrate varying signal intensities between blood and the thrombus. The corresponding R_1-maps and T_1 values are

listed below the three transverse slices. The quantitative analysis (R_1-map) shows the distribution of the relaxation rates. The T_1 value of the blood as measured in the popliteal artery was $T_1 = 1{,}422 \pm 98$ ms. Over time, the signal intensity decreased and the T_1 relaxation times increased. Figure 6, 3 indicates a higher sensitivity of the quantitative analysis compared to the results of the 3D T_1-weighted fast gradient echo. In Fig. 6, 3b, no signal enhancement can be detected inside the left popliteal vein, whereas the R_1-map still shows an enhancement within the vein.

Discussion

Besides a slight underestimation (4.2%) for long T_1 times ($T_1 = 1{,}357$ ms), the fast Look–Locker imaging scheme achieved highly accurate and reproducible T_1 measurements in phantoms of various T_1 times, covering the range of T_1 values that can be expected in human soft tissue. The underestimation of long T_1 relaxation times can be explained with the not fully recovered longitudinal magnetization after 4 s. This yields to an error in the calculation of T_1 using Eq. (2). However, the clinical application of 3D T_1-mapping using Look–Locker does require a compromise between total scan time and accuracy of the measurement. The use of longer scan times does increases the risk of patient movement during the scan.

The in vivo part of this study, in which quantitative T_1-maps of volunteers were obtained, also achieved a good reproducibility for the fast T_1 measurement technique. The resolution of the T_1-maps in patients was high enough for relatively small anatomical structures such as resolving thrombi to be identified. T_1 values derived for normal blood and various other tissues compared favorable to those reported in the literature for measurements at 1.5 T [29,39].

For the patient feasibility study, the presence of DVT was confirmed by MRI in all patients. Acute thrombi are highlighted on the T_1-weighted images including a suppression of venous and arterial blood without any perceptible reduction in the contrast of the acute thrombi. However, with this imaging method, resolving thrombi with longer T_1 relaxation times are more difficult to detect especially at higher heart rates. The average heart rate of all patients was 72 beats per minute (bpm). The Fleckenstein-equation [37] shows that the performance of an inversion pulse every 833 ms (72 bmp) results in a decreased difference of signal intensity between a thrombus with a T_1 of 950 ms and the surrounding blood ($T_1 = 1{,}400$ ms) of only 4%. In contrast to this, the T_1-mapping sequence performed the inversion pulse every 5.3 s.

In all 4 patients, the multislice bSSFP images always resulted in the largest thrombus size and remained for much longer compared to the 3D T_1-weighted fast gradient echo and the T_1-mapping sequences. The reason for this is that the multislice bSSFP sequence is flow sensitive and can only distinguish between flowing and non-flowing or very slow flowing tissue. Therefore, very slow flowing blood can mimic a thrombus inside the vein and can lead to an overestimation and false diagnosis of the thrombus volume. The flow sensitivity of the sequence is parameter dependent and defined by the slice thickness and the TR. In comparison, the T_1-weighted and T_1-mapping sequences can visualize the thrombus based on tissue property (amount of methemoglobin). Although the flow-sensitive multislice bSSFP sequence shows a very high sensitivity in detecting a small occlusion, it does not provide any tissue characteristics.

In agreement with previous studies, the area of acute thrombus in all patients was visualized on native images as a region of decreased T_1 times. To our knowledge, this is the first time that an absolute measurement of the T_1 relaxation time in patients with acute DVT has been performed in vivo. This presents a new perspective for the analysis of resolving thrombi, which heretofore could only be quantified in terms of their spatial extent, whereas the degree of signal changes as compared to normal blood could only be differentiated as 'present' or 'not present'.

Over time, the size of each thrombus decreased on all three different imaging sequences (T_1-weighted fast gradient echo, multislice bSSFP, T_1-mapping). After 6 months, the T_1 relaxation time returned to the normal T_1 relaxation time of blood, which coincided with the advised period of anticoagulation for acute DVT by international consensus [40].

Conclusion

With the use of a fast T_1-Look–Locker sequence, highly accurate and reproducible measurements of a wide range of T_1 were performed in vivo. High-resolution T_1-maps were acquired in vivo yielding T_1 values for a number of different tissues, including skeletal muscle, normal blood, and subcutaneous fat, which agree well with values found in the literature. Signal changes in areas with acute DVT were quantified. The use of a Look–Locker method provides a promising tool for the measurement of T_1 of DVT under clinical conditions.

The comprehensive protocol and the use of the 32-channel coil allow quantitative analysis of DVT in vivo with a total scan time of less than 20 min. The local T_1 quantification of the thrombus can provide information about tissue characteristics. Such a quantitative imaging method may be valuable in studying the factors that influence natural resolution and in evaluating the effects of treatments that enhance this process.

References

1. Beyer J, Schellong S (2005) Deep vein thrombosis: current diagnostic strategy. Eur J Intern Med 16:238–246
2. Fraser DGW, Moody AR, Morgan PS, Martel AL, Davidson I (2002) Diagnosis of lower-limb deep venous thrombosis:

a prospective blinded study of magnetic resonance direct thrombus imaging. Ann Int Med 136:89–98
3. Takatsu H, Fujiwara H (1999) Imaging of the "active" thrombus: can it be a new gold standard for acute deep vein thrombosis. J Nucl Med 40:2036–2037
4. Subramaniam RM, Heath R, Chou T, Cox K, Davis G, Swarbrick M (2005) Deep venous thrombosis: withholding anticoagulation therapy after negative complete lower limb US findings. Radiology 237:348–352
5. Spritzer CE, Arata MA, Freed KS (2001) Isolated pelvic deep venous thrombosis: relative frequency as detected with MR imaging. Radiology 219:521–525
6. Aschauer M, Deutschmann HA, Stollberger R, Hausegger KA, Obernosterer A, Schollnast H, Ebner F (2003) Value of a blood pool contrast agent in MR venography of the lower extremities and pelvis: preliminary results in 12 patients. Magn Reson Med 50:993–1002
7. Kanne JP, Lalani TA (2004) Role of computed tomography and magnetic resonance imaging for deep venous thrombosis and pulmonary embolism. Circulation 109:I15–I21
8. Lebowitz JA, Rofsky NM, Krinsky GA, Weinreb JC (1997) Gadolinium-enhanced body MR venography with subtraction technique. Am J Roentgenol 169:755–758
9. Wang MS, Haynor DR, Wilson GJ, Maki JH (2006) Intravascular hematocrit layering in equilibrium phase contrast-enhanced MR angiography of the peripheral vasculature. J Magn Reson Imaging 24:1393–1400
10. Kelly J, Hunt BJ, Moody A (2003) Magnetic resonance direct thrombus imaging: a novel technique for imaging venous thromboemboli. Thromb Haemostasis 89:773–782
11. Moody AR (1997) Direct imaging of deep-vein thrombosis with magnetic resonance imaging. Lancet 350:1073–1073
12. Moody AR (2003) Magnetic resonance direct thrombus imaging. J Thromb Haemostasis 1:1403–1409
13. Moody AR, Pollock JG, O'Connor AR, Bagnall M (1998) Lower-limb deep venous thrombosis: direct MR imaging of the thrombus. Radiology 209:349–355
14. Spuentrup E, Buecker A, Stuber M, Gunther RW (2001) MR-venography using high resolution true-FISP. Röfo 173:686–690
15. Rapoport S, Sostman HD, Pope C, Camputaro CM, Holcomb W, Gore JC (1987) Venous clots—evaluation with MR imaging. Radiology 162:527–530
16. Moody AR, Morgan PS, Fraser D, Hunt BJ (2000) T1 reducing properties of methaemoglobin: application to direct MR thrombus imaging. In: Proceedings of the ISMRM 8th Scientific Meeting, vol 1
17. McGuinness CL, Humphries J, Waltham M, Burnand KG, Collins M, Smith A (2001) Recruitment of labelled monocytes by experimental venous thrombi. Thromb Haemostasis 85:1018–1024
18. Modarai B, Burnand KG, Humphries J, Waltham M, Smith A (2005) The role of neovascularisation in the resolution of venous thrombus. Thromb Haemostasis 93:801–809
19. Schmitz SA, O'Regan DP, Gibson D, Cunningham C, Fitzpatrick J, Allsop J, Larkman DJ, Hajnal JV (2006) Magnetic resonance direct thrombus imaging at 3T field strength in patients with lower limb deep vein thrombosis: a feasibility study. Clin Radiol 61:282–286
20. Westerbeek RE, Rooden CJ, Tan M, Van Gils APG, Kok S, Bats MJ, De Roos A, Huisman MV (2008) Magnetic resonance direct thrombus imaging of the evolution of acute deep vein thrombosis of the leg. J Thromb Haemostasis 6:1087–1092
21. Hahn EL (1949) An accurate nuclear magnetic resonance methods for measuring spin-lattice relaxation times. Phys Rev 76:145–146
22. Deoni SCL, Peters TM, Rutt BK (2004) Determination of optimal angles for variable nutation proton magnetic spin-lattice, T-1, and spin-spin, T-2, relaxation times measurement. Magn Reson Med 51:194–199
23. Deoni SCL, Rutt BK, Peters TM (2003) Rapid combined T-1 and T-2 mapping using gradient recalled acquisition in the steady state. Magn Reson Med 49:515–526
24. Homer J, Beevers MS (1985) Driven-equilibrium single pulse observation of T1 relaxation—a reevaluation of a rapid new method for determining NMR spin-lattice relaxation times. J Magn Reson 63:287–297
25. Preibisch C, Deichmann R (2009) Influence of RF spoiling on the stability and accuracy of T-1 mapping based on spoiled FLASH with varying flip angles. Magn Reson Med 61:125–135
26. Look DC, Locker DR (1970) Time saving in measurement of NMR and EPR relaxation times. Rev Sci Instrum 41:250–251
27. Deichmann R, Haase A (1992) Quantification of T1 values by SNAPSHOT-FLASH NMR imaging. J Magn Reson 96:608–612
28. Simonetti OP, Finn JP, White RD, Laub G and Henry DA (1994) "Black blood" T2-weighted inversion-recovery MR imaging of the heart. 1994 RSNA Scientific Assembly, pp 49–57
29. Stanisz GJ, Odrobina EE, Pun J, Escaravage M, Graham SJ, Bronskill MJ, Henkelman RM (2005) T-1, T-2 relaxation and magnetization transfer in tissue at 3T. Magn Reson Med 54:507–512
30. Arnold JFT, Fidler F, Wang T, Pracht ED, Schmidt M, Jakob PM (2004) Imaging lung function using rapid dynamic acquisition of T-1-maps during oxygen enhancement. Magn Reson Mat Phys Biol Med 16:246–253
31. Deichmann R, Hahn D, Haase A (1999) Fast T-1 mapping on a whole-body scanner. Magn Reson Med 42:206–209
32. Gowland P, Mansfield P (1993) Accurate measurement of T1 in vivo in less than 3 seconds using echo-planar imaging. Magn Reson Med 30:351–354
33. Haase A (1990) Snapshot FLASH MRI—applications to T1, T2, and chemical-shift imaging. Magn Reson Med 13:77–89
34. Shah NJ, Zaitsev M, Steinhoff S, Zilles K (2001) A new method for fast multislice T-1 mapping. Neuroimage 14:1175–1185
35. Scheffler K, Lehnhardt S (2003) Principles and applications of balanced SSFP techniques. Eur Radiol 13:2409–2418
36. Klein WM, Bartels LW, Bax L, van der Graaf Y, Mali W (2003) Magnetic resonance imaging measurement of blood volume flow in peripheral arteries in healthy subjects. J Vasc Surg 38:1060–1066
37. Fleckenstein JL, Archer BT, Barker BA, Vaughan JT, Parkey RW, Peshock RM (1991) Fast short tau inversion recovery MR imaging. Radiology 179:499–504
38. Bland JM, Altman DG (1986) Statistical-methods for assessing agreement between 2 methods of clinical measurement. Lancet 1:307–310
39. Gold GE, Han E, Stainsby J, Wright G, Brittain J, Beaulieu C (2004) Musculoskeletal MRI at 3.0T: relaxation times and image contrast. Am J Roentgenol 183:343–351
40. Huisman MV (2000) Recurrent venous thromboembolism: diagnosis and management. Curr Opin Pulm Med 6:330–334